

Crystal structure and luminescence of Na[Eu(DCTA)·H₂O]·4H₂O (DCTA = *trans*-cyclohexane-1,2-diylidinitrilotetraacetate)

Jun-Gill Kang,^{*a} Soo-Kyung Yoon,^a Youngku Sohn,^a Jong-Goo Kim,^b Youn-Doo Kim^a and Il-Hwan Suh^c

^a Department of Chemistry, Chungnam National University, Taejeon, 305-764, Korea.

E-mail: jgkang@hanbat.chungnam.ac.kr

^b Korea Atomic Energy Research Institute, Taejeon, 302-353, Korea

^c Department of Physics, Chungnam National University, Taejeon, 305-764, Korea

Received 6th October 1998, Accepted 1st March 1999

The crystal structure and the luminescence of the complex Na[Eu(DCTA)·H₂O]·4H₂O (DCTA = *trans*-cyclohexane-1,2-diylidinitrilotetraacetate) have been determined. In the structure the Eu^{III} is co-ordinated by two nitrogen atoms and four terminal oxygen atoms of two iminodiacetate groups, and two water oxygen atoms which bridge two adjacent Eu^{III}. When the crystals are excited by UV light they produce a very characteristic luminescence responsible for the ⁵D₀ → ⁷F_J (J = 0, 1, 2, 3, 4) transitions. The energy-level scheme of the ⁷F_J states and detailed assignments for the observed luminescence lines have been proposed by phenomenological simulation in the framework of the free-ion and crystal-field Hamiltonians. Although an additional correction to the free-ion model is needed for the barycenter shifting due to the complexation, the set of refined crystal-field parameters under C_{2v} site symmetry satisfactorily reproduces the fine splitting of the luminescence lines in the ⁵D₀ → ⁷F_J (J = 0, 1, 2, 3, 4) transitions. The behavior of the maximum splitting of the ⁷F₁ manifold is also discussed in terms of a scalar crystal-field strength parameter.

Introduction

There has been much interest in the optical properties of trivalent lanthanide ions because of their hypersensitivity to the ligand environment.¹⁻⁴ Among these ions, the europium ion is useful for studying the nature of metal co-ordination in various systems, owing to its non-degenerate emitting ⁵D₀ state. These studies include determining local symmetry and the number of different co-ordination sites, probing the structure of biological molecules, and understanding stereochemical properties.⁵ Most of these studies have been performed in solution. Unlike the case in solution, in the solid state the luminescence spectrum of the europium(III) complex attributed to the ⁵D₀ → ⁷F_J (J = 0, 1, 2, 3, 4) transitions consists of groups of remarkably sharp lines. The crystal-field potential plays a key role in the optical process, which is characterized by the site symmetry in the complex.⁶

Using the luminescence properties of Eu^{III}, the co-ordination chemistry of the DCTA ligand (*trans*-cyclohexane-1,2-diylidinitrilotetraacetate) has been studied to obtain kinetic information on the equilibrium dynamics of complexation⁷ and to evaluate it as a nuclear magnetic resonance shift reagent.⁸ Until now, however, the crystal structure and the optical properties of the Eu^{III}-DCTA complex have not been reported. This study is designed to provide a detailed characterization of the molecular structure and luminescence properties of it. The luminescence and the electronic energy-level structure of the ⁷F_J states are assigned by simulating the phenomenological crystal-field splitting.

Experimental

Growth of single crystals and composition analysis

The EuCl₃·6H₂O and *trans*-cyclohexane-1,2-diylidinitrilotetraacetic acid (HDCTA) were of analytical grade (Aldrich) and used without further purification. The mother solution was prepared by mixing solutions of 0.50 M Eu^{III} and 0.50 M HDCTA. The container holding the mother solution was

placed in a sealed flask surrounded by a water jacket. Thermostatic control better than 0.010 K was achieved with a Fisher isotemperature refrigerated circulator. While the crystals were growing the pH of the solution was maintained at nearly 7.0. Needle-shape crystals were isolated from the mother solution by lowering the temperature of the solution from the equilibrium saturation temperature. Several samples were grown under identical conditions for the structural analysis and optical measurements.

The quantitative analysis of Na⁺ and Eu³⁺ ions was conducted on a Jovin-Yvon ICP spectrophotometer and the analyses of the total organic carbon, nitrogen and hydrogen were made on an EA 1110 Automatic Elemental Analyzer. The relative molar amounts found were Na⁺:Eu³⁺:DCTA = 1.5:1.2:1. A potentiometric analysis also showed that there was no chloride ion in the crystals. The TG/DTA spectra of the crystals were recorded up to 300 °C with a Setaram TGA-92 instrument. Weight loss occurred at two distinct steps in the temperature range from 70 to 190 °C. Excluding the possibility of thermal decomposition of the ligand in this temperature range, the weight loss below 100 °C may result from the evaporation of solvated water molecules, while that above 100 °C could arise from evaporation of co-ordinated water molecules. Around 142 °C the weight dropped 1.40 mg from 22.16 mg. This weight loss results in a 1:1 molar ratio of H₂O:NaEu(DCTA). In other words, one water molecule is co-ordinated to each Eu^{III}. The number of water molecules associated with the crystal was also confirmed by X-ray diffraction analysis. The quantitative analyses showed that the formula of the Eu/DCTA crystals was Na[Eu(DCTA)·H₂O]·4H₂O.

Solution and refinement of the crystal structure

The structure of the complex was determined at 15 °C. A colorless single crystal 0.36 × 0.5 × 0.4 mm in size was coated with lacquer, because of its instability in air, and mounted on an Enraf-Nonius CAD4 diffractometer equipped with graphite monochromated Mo-K α radiation. The cell parameters and

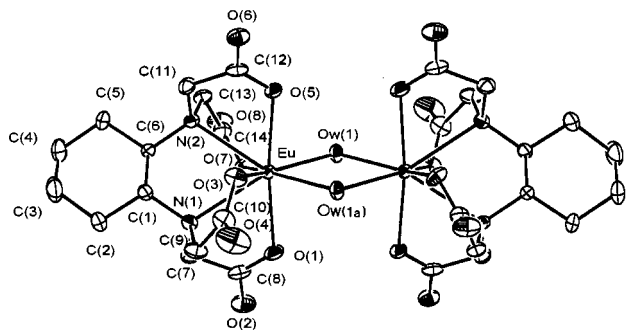


Fig. 1 An ORTEP drawing of $[\text{Eu}(\text{DCTA})\cdot\text{H}_2\text{O}]_2^{2-}$ and the atom-labeling scheme. The displacement ellipsoids are drawn at the 40% probability level and hydrogen atoms are omitted for clarity.

orientation matrix were determined from the least-squares fit of 25 accurately centered reflections with θ angles between 11.39 and 14.56°. The intensity data were collected in the ω - 2θ scan mode to a maximum 2θ of 50.10°. Three standard reflections (3 5 2, -12 4 -2, -15 -1 -2) were measured every 240 min and the intensities of the standards remained constant within 2% throughout data collection. Of the 3787 unique reflections measured, 3186 were used in the subsequent structure analysis. The SDA package supplied by Nonius was used to correct the intensities from Lorentz-polarization factors, but no absorption correction was applied.

The structure was solved by direct methods using SHELXS 86^{9a} and refined by a full-matrix least-squares refinement on F using SHELXL 97.^{9b} All of the non-H atoms were refined anisotropically, but only one water molecule was involved in the isotropic refinement because of its very small thermal vibration. All the hydrogen atoms except those in water were placed in calculated positions attached to the appropriate carbon atom. The final reliability factors for the 3287 unique observed reflections [$F_o > 4\sigma(F_o)$] were $R = 0.0248$ and $R' = 0.0612$. Crystal data and refinement results are summarized in Table 1.

CCDC reference number 186/1364.

See <http://www.rsc.org/suppdata/dt/1999/1467/> for crystallographic files in .cif format.

Optical measurements

For luminescence and excitation spectra measurements a needle-shaped crystal was placed on the cold finger of an Oxford CF-1104 cryostat using silicon grease. The light from an Oriol 1000 W xenon lamp (working power, 400 W) was passed through an Oriol MS257 monochromator and focused on the sample. The luminescence was detected at right angles with an ARC 0.5 m Czerny-Turner monochromator equipped with a cooled Hamamatsu R-933-14 PM tube. The optical arrangement for measuring the excitation spectrum is the same as for the luminescence measurement. In addition, the luminescence spectrum of the aqueous solution was measured on an Edinburgh FS-900 spectrofluorometer.

Results and discussion

Crystal structure

The Eu-DCTA complex crystallizes in the monoclinic space group $P2_1/c$ ($Z = 4$). The ORTEP¹⁰ drawing of this molecular unit is shown in Fig. 1. Selected bond lengths and angles are given in Table 2. The DCTA has two iminodiacetate ions substituted at positions 1 and 2 of the cyclohexane ring. In each iminodiacetate group a nitrogen atom and two oxygen atoms with negative charges are co-ordinated to the Eu^{III} . In the $[\text{Eu}(\text{DCTA})]^-$ complex the DCTA acts as a hexadentate ligand and forms five five-membered chelate rings through the two nitrogen atoms. Four rings consist of the nitrogen and oxygen

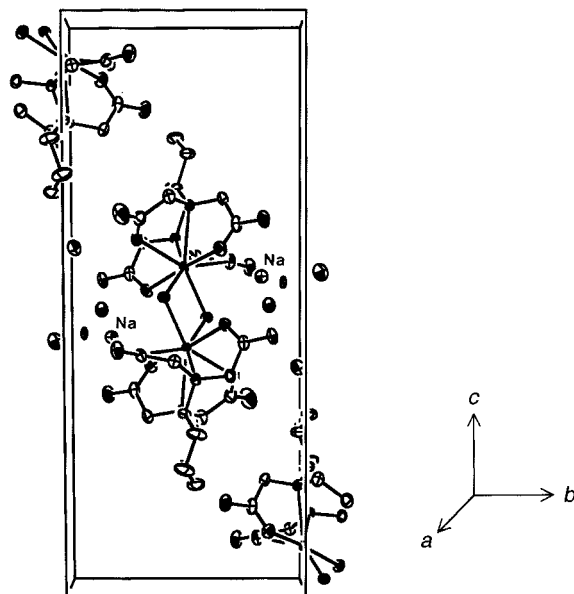


Fig. 2 A unit-cell packing diagram of $\text{Na}[\text{Eu}(\text{DCTA})\cdot\text{H}_2\text{O}]\cdot 4\text{H}_2\text{O}$. The origin is at the lower left, the b axis is horizontal and the a axis is vertical. Hydrogen atoms are omitted for clarity. The two water oxygen atoms bridge two adjacent europium(III) ions.

atoms of each iminodiacetate group and the fifth consists of two carbon atoms of the cyclohexane ring and two nitrogen atoms. The two iminodiacetate groups are bridged *via* an N1-Eu-N2 bond. The two Eu-N bonding distances are almost identical [Eu-N1 2.644(3), Eu-N2 2.627(3) Å]. The angle N1-Eu-N2 is 67.70(11)°.

Of the four Eu-O bonds, one [Eu-O3 2.401(3) Å] is a little longer than the others [Eu-O1 2.370(3), Eu-O5 2.387(3), Eu-O7 2.390(3) Å]. The shorter distance may cause the N-Eu-O angle to widen in order to reduce the electron repulsion between the two bonds. Conversely, of the two bond angles formed from the N1 atom, N1-Eu-O1 [64.40(11)°] is a little wider than N1-Eu-O3 [63.31(11)°]. In the two groups formed by the other iminodiacetate group, the two bond angles are almost identical [N2-Eu-O5 64.55(10), N2-Eu-O7 65.01(10)°].

Five water molecules are involved in each molecular unit. For them, the characteristic features in the structure can be found in the two water molecules labeled OW1 and OW1(a). Here, OW1(a) is generated by the symmetry transformation $1 - x$, $1 - y$ and $1 - z$. The distance between Eu and OW1(a) is almost the same as that between Eu and OW1 [Eu-OW1(a) 2.336(3), Eu-OW1 2.342(3) Å]. This suggests that OW1 could be co-ordinated to both Eu and Eu ($1 - x$, $1 - y$, $1 - z$). It can be presumed that the two water molecules may be directly co-ordinated to two adjacent europium(III) ions with almost identical bond lengths of 2.340 Å *via* Eu-O-Eu bonding. In other words, two molecular $[\text{Eu}(\text{DCTA})]^-$ units may be linked through two water molecules, resulting in a dimeric form, as shown in Fig. 1. The rest of the water molecules are aggregated between the layers, as shown in Fig. 2.

Luminescence and excitation spectra

The luminescence spectrum of the $[\text{Eu}(\text{DCTA})]^-$ crystals excited at 395 nm was measured at wavelengths from 575 to 725 nm at room temperature and at 78.8 K. There was no significant difference between the spectra measured at the two temperatures. It was found that with decreasing temperature the bands become sharper and more intense. This suggests that the molecular symmetry of the crystals is well conserved from room temperature to 78.8 K. Fig. 3 shows the luminescence spectrum measured at 78.8 K. For comparison, the luminescence spectra of $\text{Eu}^{3+}(\text{aq})$ and a 1:1 molar ratio solution of

Table 1 Crystallographic data and refinement for Na[Eu(DCTA)·H₂O]·4H₂O

Chemical formula	C ₁₄ H ₂₈ EuN ₂ NaO ₁₃
<i>M</i>	607.33
Cell setting	Monoclinic
Space group	<i>P</i> 2 ₁ / <i>c</i>
<i>a</i> /Å	8.612(2)
<i>b</i> /Å	9.9105(16)
<i>c</i> /Å	24.250(6)
β /°	98.38(2)
<i>V</i> /Å ³	2047.6(8)
<i>Z</i>	4
<i>F</i> (000)	1216
<i>D</i> _x g cm ⁻³	1.970
λ (Mo-K α)/Å	0.71069
μ /cm ⁻¹	31.56
<i>R</i>	0.0248
<i>R</i> '	0.0612
<i>S</i>	1.143
($\Delta I\rho$) _{max} , ($\Delta I\rho$) _{min} /e Å ⁻³	0.649, -0.661

Eu^{III}:DCTA were also measured at room temperature. The 618 nm emission band, responsible for the ⁵D₀ → ⁷F₂ transition, was markedly intensified by complexation with DCTA. As the complex changed from aqueous to crystalline, characteristic band splitting was observed in most of the bands of the ⁵D₀ → ⁷F_{*J*} (*J* = 1, 2, 3, 4) transitions. The number of bands revealed that the (2*J* + 1) fold degeneracy of the ⁷F_{*J*} (*J* = 1, 2, 3, 4) states is removed by the crystal-field potential.

The excitation spectrum of the 610.9 nm emission from the [Eu(DCTA)]⁻ crystals was also measured at 78.8 K. Fig. 4 shows the sharp lines caused by transitions within the 4f⁶ ground configuration. The band splitting of the excited states also appeared in the excitation spectrum. Under an identical crystal field potential, however, the lifting of the degeneracy of the excited states was less than in the case of the ground ⁷F_{*J*} states. The characteristic feature in the excitation spectrum can be found in the 465 nm band, which is attributed to the ⁷F₀ → ⁵D₂ transition. It is well accepted that of the three intensity parameters, Ω_2 reflects the sensitivity to the ligand environment if the matrix element *U*⁽²⁾ is not very small, compared with the values *U*⁽⁴⁾ and *U*⁽⁶⁾.¹¹ For transitions originating from the ⁷F₀ state, only the ⁷F₀ → ⁵D₂ has a non-zero *U*⁽²⁾ matrix element. This transition is sensitive to the ligand environment, but has not drawn special attention because of the small value of the *U*⁽²⁾ matrix element.¹² It can be seen from the excitation spectrum that the oscillator strength of this transition is comparable to that of the ⁷F₀ → ⁵L₆ transition which is the strongest in the UV and visible region. Enhancement of the oscillator strength of the ⁷F₀ → ⁵D₂ transition has been observed in some polycarboxylate complexes.^{13,14} This may indicate that DCTA offers strong chemical binding ability *via* the two iminodiacetate groups.

The identification of some of the luminescence remains ambiguous due to superposition of several transitions originating from different emitting levels, *e.g.* ⁵D₁ and/or ⁵D₂. These bands are difficult to separate from the ⁵D₀ → ⁷F_{*J*} transition bands. For some europium(III) complexes, one extra, moderately intense, band attributed to the ⁵D₁ → ⁷F₃ transition appears on the high-energy side of the ⁵D₀ → ⁷F₁ transition. This problem is solved by selective excitation at the ⁵D₀ level. The luminescence spectrum was measured in the 590–600 nm region with 582 nm excitation. As shown in Fig. 5, 582 nm excitation also produces the three luminescence bands. This demonstrates that the three bands in this wavelength region originate from the ⁵D₀ state. Very weak, broad bands appeared on the low-energy side of the hypersensitive ⁵D₀ → ⁷F₂ transition. It can be seen from the expanded scale of the spectrum that these bands consist of multiple lines. Taking into account the band structure and the characteristic feature of the ⁵D₀ → ⁷F₂ transition, these bands may be classified as arising

Table 2 Selected bond lengths (Å) and angles (°) in Na[Eu(DCTA)·H₂O]·4H₂O^a

Eu–OW1(a)	2.336(3)	N(1)–C(7)	1.484(5)
Eu–OW1	2.342(3)	N(1)–C(9)	1.490(5)
Eu–O(1)	2.370(3)	N(1)–C(1)	1.499(5)
Eu–O(3)	2.401(3)	N(2)–C(11)	1.474(5)
Eu–O(5)	2.387(3)	N(2)–C(13)	1.483(5)
Eu–O(7)	2.390(3)	N(2)–C(6)	1.506(5)
Eu–N(1)	2.644(3)	C(1)–C(6)	1.530(6)
Eu–N(2)	2.627(3)	C(1)–C(2)	1.556(6)
O(1)–C(8)	1.271(6)	C(2)–C(3)	1.536(7)
O(2)–C(8)	1.240(6)	C(3)–C(4)	1.496(9)
O(3)–C(10)	1.263(6)	C(4)–C(5)	1.534(7)
O(4)–C(10)	1.233(6)	C(5)–C(6)	1.535(6)
O(5)–C(12)	1.260(5)	C(7)–C(8)	1.525(7)
O(6)–C(12)	1.246(5)	C(9)–C(10)	1.541(7)
O(7)–C(14)	1.286(5)	C(11)–C(12)	1.545(6)
O(8)–C(14)	1.223(5)	C(13)–C(14)	1.524(6)
OW1(a)–Eu–OW1	69.41(12)	C(7)–N(1)–Eu	105.7(2)
OW1(a)–Eu–O(1)	82.81(11)	C(9)–N(1)–Eu	104.3(2)
OW1–Eu–O(1)	91.97(11)	C(1)–N(1)–Eu	113.3(2)
OW1(a)–Eu–O(7)	141.36(10)	C(11)–N(2)–C(13)	110.7(3)
OW1–Eu–O(7)	76.49(11)	C(11)–N(2)–C(6)	113.6(3)
O(1)–Eu–O(7)	80.69(11)	C(13)–N(2)–C(6)	108.6(3)
OW1(a)–Eu–O(5)	89.54(10)	C(11)–N(2)–Eu	107.6(2)
OW1–Eu–O(5)	83.66(11)	C(13)–N(2)–Eu	103.0(2)
O(1)–Eu–O(5)	172.15(10)	C(6)–N(2)–Eu	112.9(2)
O(5)–Eu–O(7)	104.50(11)	N(1)–C(1)–C(6)	111.1(3)
OW1(a)–Eu–O(3)	77.56(11)	N(1)–C(1)–C(2)	112.5(3)
OW1–Eu–O(3)	142.28(11)	C(6)–C(1)–C(2)	110.7(4)
O(1)–Eu–O(3)	101.67(11)	C(3)–C(2)–C(1)	110.9(4)
O(5)–Eu–O(3)	78.25(11)	C(4)–C(3)–C(2)	111.4(4)
O(7)–Eu–O(3)	140.06(11)	C(3)–C(4)–C(5)	109.1(5)
OW1(a)–Eu–N(2)	149.70(11)	C(4)–C(5)–C(6)	111.5(4)
OW1–Eu–N(2)	119.45(11)	N(2)–C(6)–C(1)	111.8(3)
O(1)–Eu–N(2)	123.28(11)	N(2)–C(6)–C(5)	111.7(3)
O(5)–Eu–N(2)	64.55(10)	C(1)–C(6)–C(5)	111.3(4)
O(7)–Eu–N(2)	65.01(10)	N(1)–C(7)–C(8)	111.0(4)
O(3)–Eu–N(2)	81.74(11)	O(2)–C(8)–O(1)	124.3(5)
OW1(a)–Eu–N(1)	119.98(10)	O(2)–C(8)–C(7)	117.4(4)
OW1–Eu–N(1)	151.14(11)	O(1)–C(8)–C(7)	118.3(4)
O(1)–Eu–N(1)	64.40(11)	N(1)–C(9)–C(10)	111.2(4)
O(5)–Eu–N(1)	121.61(11)	O(4)–C(10)–O(3)	126.0(5)
O(7)–Eu–N(1)	83.17(11)	O(4)–C(10)–C(9)	117.5(4)
O(3)–Eu–N(1)	63.31(11)	O(3)–C(10)–C(9)	116.5(4)
N(2)–Eu–N(1)	67.70(11)	N(2)–C(11)–C(12)	111.4(3)
Eu(a)–OW1–Eu	110.59(12)	O(6)–C(12)–O(5)	125.0(4)
C(8)–O(1)–Eu	120.2(3)	O(6)–C(12)–C(11)	117.2(4)
C(10)–O(3)–Eu	115.0(3)	O(5)–C(12)–C(11)	117.9(4)
C(12)–O(5)–Eu	119.7(3)	N(2)–C(13)–C(14)	111.4(3)
C(14)–O(7)–Eu	120.6(3)	O(8)–C(14)–O(7)	123.3(4)
C(7)–N(1)–C(9)	109.6(3)	O(8)–C(14)–C(13)	120.2(4)
C(7)–N(1)–C(1)	114.3(3)	O(7)–C(14)–C(13)	116.5(4)
C(9)–N(1)–C(1)	109.1(3)		

^a Symmetry transformation used to generate equivalent atoms: (a) $-x + 1, -y + 1, -z + 1$.

from the ⁵D₁ → ⁷F₄ transition. Except for this transition, all the bands, shown in Fig. 3, can be attributed to the ⁵D₀ → ⁷F_{*J*} transitions. The analysed wavenumbers of these transitions are listed in Table 3.

The extent to which the (2*J* + 1) degeneracy is removed depends upon the site symmetry of the europium(III) ion. Some possible site symmetries for the Eu^{III} in the DCTA complex would be C_{2h}, C_{2v} or C₂. For the Eu³⁺ ion all the transitions from the ⁵D₀ to the ⁷F_{*J*} states except *J* = 1 are allowed by the electric dipole moment. Here, the transition to the ⁷F₁ state is characterized mostly by the magnetic dipole moment. Taking into account the selection rules, under any C_{2h} site symmetry, no characteristic luminescence bands are observed in the ⁵D₀ → ⁷F_{*J*} (*J* = 0, 2, 3, 4) transitions. Under C₂ site symmetry, the Eu^{III} may produce the maximum number of (2*J* + 1) lines in the transitions from the ⁵D₀ state to any of the ⁷F_{*J*} states. Consequently, the number of observed bands in the transitions from the ⁵D₀ to the ⁷F_{3,4} states leads us to choose C_{2v} for the site

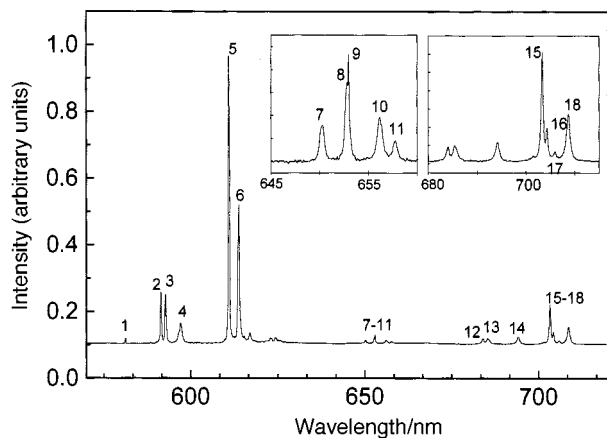


Fig. 3 Luminescence spectrum of $[\text{Eu}(\text{DCTA})]^-$ complex in the crystalline state excited at 395 nm ($T = 78.8$ K).

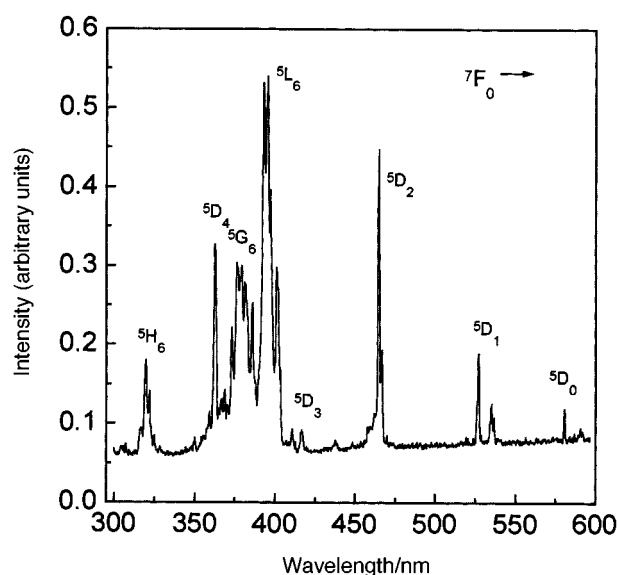


Fig. 4 Excitation spectrum of the 610.9 nm emission from $[\text{Eu}(\text{DCTA})]^-$ in the crystalline state.

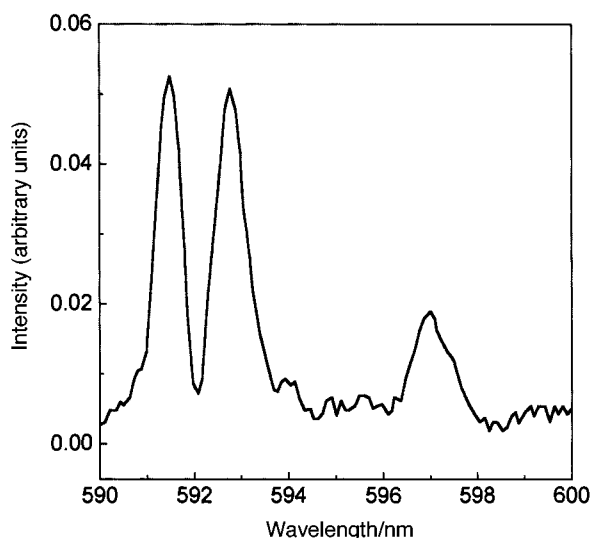


Fig. 5 Emission spectrum in the ${}^5\text{D}_0 \rightarrow {}^7\text{F}_1$ region from $[\text{Eu}(\text{DCTA})]^-$ crystals excited upon the ${}^5\text{D}_0$ state ($\lambda_{\text{ex}} = 582$ nm and $T = 78.8$ K).

symmetry of the Eu^{III} in the $[\text{Eu}(\text{DCTA})]^-$ complex. The ORTEP view of the molecular unit in Fig. 1 also shows that C_{2v} is quite possible for the site symmetry, taking into account the mononuclear species. If the electrostatic interaction between europium(III) ions in the dimer is comparable with the attractive

Table 3 The observed ${}^5\text{D}_0 \rightarrow {}^7\text{F}_J$ ($J = 0, 1, 2, 3, 4$) luminescence lines (cm^{-1}) of $[\text{Eu}(\text{DCTA})]^-$ ^a

No.	J	Observed	Calculated	Peak assignment ${}^5\text{D}_0(\text{A}) \rightarrow$
1	0	17204	17204	${}^7\text{F}_0(\text{A})$
2	1	16908	16918	${}^7\text{F}_1(\text{A}_2)$
3		16869	16856	${}^7\text{F}_1(\text{B}_2)$
4		16748	16746	${}^7\text{F}_1(\text{B}_1)$
5	2	16367	16367	${}^7\text{F}_2(1\text{A}_1)$
6		16291	16305	${}^7\text{F}_2(\text{B}_2)$
7	3	15379	15420	${}^7\text{F}_3(1\text{B}_2)$
8		15320	15317	${}^7\text{F}_3(1\text{B}_1)$
9		15315	15251	${}^7\text{F}_3(2\text{B}_2)$
10		15242	15227	${}^7\text{F}_3(\text{A}_1)$
11		15203	15212	${}^7\text{F}_3(2\text{B}_1)$
12	4	14621	14607	${}^7\text{F}_4(1\text{A}_1)$
13		14591	14577	${}^7\text{F}_4(1\text{B}_2)$
14		14406	14384	${}^7\text{F}_4(2\text{A}_1)$
15		14218	14220	${}^7\text{F}_4(1\text{B}_1)$
16		14198	14207	${}^7\text{F}_4(2\text{B}_1)$
17		14165	14146	${}^7\text{F}_4(2\text{B}_2)$
18		14110	14123	${}^7\text{F}_4(3\text{A}_1)$

^a An additional correction due to the complexation was made to the ${}^7\text{F}_2$ barycenter, 80 cm^{-1} with respect to the average stabilization energy, E_{av} , in eqn. (1).

interaction between Eu^{III} and the binding atoms of DCTA, the heterogeneity in the site symmetry may give rise to the complexity in the band structure in the ${}^5\text{D}_0 \rightarrow {}^7\text{F}_0$ transition. As shown in Fig. 3, a single band appeared for the ${}^5\text{D}_0 \rightarrow {}^7\text{F}_0$ transition. Accordingly, we conclude that the repulsive interaction between europium(III) ions is negligible compared with the binding interaction between Eu^{III} and DCTA. Under C_{2v} and C_2 site symmetry, the transition from the ${}^5\text{D}_0$ to the ${}^7\text{F}_0$ state gains intensity through J mixing. However, the intensity of this transition is still very low compared with those of the transitions to the ${}^7\text{F}_1$ state. This indicates that mixing of the ${}^7\text{F}_0$ with the other states could be negligible.

Simulation

For a comprehensive analysis of the observed luminescence lines, the energy-level scheme of europium(III) ions in the complex has been simulated with the aid of a complete set of Hamiltonians (1)^{6c,14} where H_{FI} is the Hamiltonian for the free

$$H = E_{\text{av}} + H_{\text{FI}} + H_{\text{CF}} \quad (1)$$

ion and H_{CF} is the crystal-field Hamiltonian (CFH) due to the ligand environment. In eqn. (1), E_{av} is the spherically symmetric part contributed by the free-ion and the crystal-field Hamiltonians. For the electronic structures of the free ion, the electrostatic and spin-orbit interactions within the f^N configurations are treated as the main part and the two-particle configuration interaction associated with the α , β and γ parameters as additional terms. Other additional terms, such as the three-particle configuration interaction and the magnetically correlated corrections, are excluded from this calculation, since they are insignificant in the simulation of the free-ion level of the Eu^{III} in the DCTA complex.

The CFH for the C_{2v} site symmetry is the same as that for the D_2 , which has been expressed in terms of the spherical tensor operators $C_q^{(k)}$ as in eqn. (2) where the CF parameters, B_q^k ,

$$H_{\text{CF}} = B_0^2 C_0^{(2)} + B_2^2 (C_2^{(2)} + C_{-2}^{(2)}) + B_0^4 C_0^{(4)} + B_2^4 (C_2^{(4)} + C_{-2}^{(4)}) + B_4^4 (C_4^{(4)} + C_{-4}^{(4)}) + B_0^6 C_0^{(6)} + B_2^6 (C_2^{(6)} + C_{-2}^{(6)}) + B_4^6 (C_4^{(6)} + C_{-4}^{(6)}) + B_6^6 (C_6^{(6)} + C_{-6}^{(6)}) \quad (2)$$

represent the expansion coefficients. Here, assuming that the crystal field potential (CFP) would not cause mixing of the ${}^7\text{F}_J$ and other electronic states due to the large energy gap, the

Table 4 Energy and crystal-field parameters (cm^{-1}) determined empirically from the luminescence spectra of $\text{Na}[\text{Eu}(\text{DCTA})\cdot\text{H}_2\text{O}]\cdot 4\text{H}_2\text{O}^a$

Parameter	Parameter		
E^1	[5940]	B_2^2	180(10)
E^2	29(0.3)	B_0^4	-1310(50)
E^3	[667]	B_2^4	-350(50)
ζ_{4f}	1330.5(0.55)	B_4^4	1170(10)
α	[20]	B_0^6	1720(20)
β	-644(0.4)	B_2^6	-1120(20)
γ	[1750]	B_4^6	40(20)
B_0^6	-510(10)	B_6^6	160(20)

^a Values in square brackets were held fixed in the fitting and values in parentheses represent uncertainties. In this work electrostatic matrix elements were specified in terms of E^1 , E^2 , E^3 which are linear combination of the F^k integrals.

matrix elements in the CFH are approximated to the problems between the $|f^N {}^7F; JJ_z\rangle$ and $|f^N {}^7F; J'J'_z\rangle$ states. According to the selection rule for the crystal quantum number (μ), the CF matrix elements between two states, $|f^N {}^7F; JJ_z\rangle$ and $|f^N {}^7F; J'J'_z\rangle$, are non-zero if the two states have the same parity in the J_z quantum number.^{6a} Introducing this selection rule to the CFH, the full 48×48 set of matrix elements can be reduced to two 24×24 sub-groups ($\mu = 0$ and ± 1).

In this work, the calculation of the 7F_J electronic states of the Eu^{III} in the complex has been carried out in two steps. First, we calculated the energy-level structure of the free-ion state with $(2J + 1)$ degeneracy by overrunning the amount of experimental data, namely the ${}^7F_{0-4}$, ${}^5D_{0-2}$, 5L_6 , 5G_6 and 5H_6 data. The calculation was carried out by the diagonalization method, in which most of the 119 states with $S \geq 1$ were included. Finally, we carried out the CF simulation on the fine structures of the 7F_J ($J = 1-6$) levels that arise from the C_{2v} crystal-field potential. The energy parameters were determined by the best fit to the observed luminescence lines responsible for the ${}^5D_0 \longrightarrow {}^7F_J$ ($J = 0, 2, 3, 4$) transitions. Specifically, the selection rule for these transitions was employed to determine the fine set of CF parameters. The energy parameters obtained are listed in Table 4.

Previously,¹⁴ we found that in simulating the luminescence lines of europium complexes a discrepancy occurred in the barycenters of the ${}^5D_0 \longrightarrow {}^7F_2$ and ${}^5D_0 \longrightarrow {}^7F_3$ transitions. Of the observed transitions, the ${}^5D_0 \longrightarrow {}^7F_2$ is the most sensitive to the complexation, while the ${}^5D_0 \longrightarrow {}^7F_3$ is the least. It has been observed that the 7F_2 state is more stabilized and the 7F_3 state is less stabilized with respect to the average shift in the 7F_J multiplets, E_{av} . Some possible improvements in theoretical energy level could be made by taking into account the Jahn–Teller stabilization¹⁶ and the nephelauxetic effect.¹¹ To date, there are no reports on the quantitative theoretical analysis of how these effects are responsible for the shift of the barycenter of each excited level. The simulation of the free-ion state of the europium(III) ion suggests that some additional terms accounting for the band energy shift in the ${}^5D_0 \longrightarrow {}^7F_2$ transition are specifically required in eqn. (1). Empirically, an additional correction of 80 cm^{-1} was made on the 7F_2 free-ion level for the fine simulation.

The calculated energy levels of the 7F_J ($J = 1-4$) states of Eu^{III} in the $[\text{Eu}(\text{DCTA})]^-$ complex are listed in Table 5. For precise assignment, their mixed $|JJ_z\rangle^*$ eigenstates were determined from the secular determinants of the CFH in combination with the calculated free-ion energy and the CF parameters obtained. The eigenstates and their irreducible representations are listed in Table 6. The eigenstates indicate that most of the luminescence lines are affected by the CF mixing between the energy levels with the same parity. The assignments for the observed luminescence lines were made in the ${}^5D_0 \longrightarrow {}^7F_J$ ($J = 0, 1, 2, 3, 4$) transitions according to the calculated wavenumbers and the selection rules in the C_{2v}

symmetry, as listed in Table 3. The set of CF parameters yields calculated wavenumbers that match very well the experimental values of most of the lines (except 7 and 9) in the ${}^5D_0 \longrightarrow {}^7F_J$ ($J = 1, 2, 3, 4$) transitions, $\sigma = 16.4 \text{ cm}^{-1}$.

Scalar CF strength parameter of the 7F_1 state

The systematic trend in the phenomenological B_q^k parameters has been grouped for a series of lanthanide(III) ions in a given host.^{15b} Similar application to lanthanide(III) complexes with DCTA is difficult, because of the lack of available data. In this study we attempted to rationalize the parameters as an indication of both the spectrum pattern and the magnitude of the maximum CF splitting of the 7F_1 state for Eu^{III} in crystals of different structures and site symmetries, since the 7F_1 state of Eu^{III} is well isolated from the other states.^{13,14,17} Here, the diagonal elements in the CFH described by eqn. (2) are characterized by B_0^k ($k = 2, 4, 6$), while the off-diagonal elements are determined by the B_q^k parameters satisfying the selection rule $\Delta J_z = |q|$. Neglecting the J mixing, the splitting of the 7F_1 state of the europium(III) ions behaves in a way directly proportional to the B_0^2 and B_2^2 parameters depending on the site symmetry. If B_0^2 is specified as a negative value, it will lower the $|1, 0\rangle$ level energy and raise the energy of the degenerate $|1, \pm 1\rangle$ levels. When B_0^2 is a positive value the opposite occurs. Furthermore, the degeneracy of the $|1, \pm 1\rangle$ level is removed by the B_2^2 parameter.

The theoretical maximum splitting, ΔE , of a given J state can be calculated from the B_q^k parameters by using the so-called scalar crystal field strength parameter, N_v , which is given by¹⁸ eqn. (3) and represents the distance in the space spanned by the

$$N_v = \left[\sum_{k,q} (B_q^k)^2 \left(\frac{4\pi}{2k+1} \right) \right]^{1/2} \quad (3)$$

spherical harmonics, Y_q^k . The theoretical formula for the maximum splitting of a given J state has been developed from the relationship between the root-mean-square deviation of the energies of a number of levels and the projection of the spherical tensor under the CFP onto the subspace of the free-ion state. The maximum splitting for a small J value is given by^{18b} eqn. (4) where g is the degeneracy of the J level ($g_a = g$ for

$$\Delta E = \left(\frac{g_a}{g\pi p} \right)^{1/2} \left| \left\langle J \left\| \sum_i C^{(k)}(i) \right\| J \right\rangle \right|_{N_v} \quad (4)$$

an integer J , $g_a = g/2$ for a half-integer J) and the index i runs over the $4f$ electrons. The reduced matrix elements of the spherical tensor operator can easily be evaluated *via* the sum of the unit tensor. The quantity p is the sum of the square deviations from the center of gravity run over each level, in units of $\Delta E/2$. Letting a_i be a fraction of the level giving the splitting within the interval ΔE , then p is given by $(1 + a_2^2 + a_3^2 + \dots + a_{g-2}^2 + 1)$. Since the J mixing of the 7F_1 state of Eu^{III} is nearly negligible, we confined the theoretical calculation of the maximum splitting to the 7F_1 state. For the 7F_1 state the calculation is simplified to the case of $k = 2$ in eqns. (3) and (4). The theoretical and experimental splittings of the 7F_1 state for europium(III) complexes with some interesting polycarboxylate ligands are listed in Table 6. There is quite good agreement between the theoretical and experimental ΔE values. Here, not only the B_q^2 ($q = 0, 2$) but also the B_4^4 parameter determine the energies of the 7F_1 sub-levels. The B_4^4 parameter in off-diagonal elements of the CFH causes the 7F_1 state to mix with other J states. For the $[\text{Eu}(\text{DCTA})]^-$ complex, the J mixing of the 7F_1 with the 7F_3 state may cause some disagreement between the theoretical and experimental splitting. Overall, this shows that the precise B_q^k parameters are very useful as crystal field probes for the 7F_1 state of europium(III) ions in different

Table 5 Energies and major $|J, J_z\rangle$ components calculated by the crystal-field effect for the 7F_J multiplets ($J = 0, 1, 2, 3, 4$)

Level	Energy/ cm ⁻¹	Major component
A(7F_0)	0	1.00 0, 0)
A ₂ (7F_1)	286	1.00 1, 0)
B ₂ (7F_1)	348	0.69 1, -1)+0.69 1, 1)+0.07 2, -1)+0.07 2, 2)-0.08 3, -3)+0.08 3, -1)+0.08 3, 1)-0.08 3, 3)
B ₁ (7F_1)	458	0.70 1, -1)-0.70 1, 1)+0.08 3, -1)-0.08 3, 1)+0.06 3, -3)+0.07 3, -1)-0.07 3, 1)-0.06 3, 3)
B ₁ (7F_2)	809	0.09 1, -1)+0.09 1, 1)+0.70 2, -1)+0.7 2, -1)
1A ₁ (7F_2)	837	0.68 2, -2)-0.12 2, 0)+0.68 2, 2)+0.18 3, -2)-0.18 3, 2)
B ₂ (7F_2)	899	0.08 1, -1)-0.08 1, 1)+0.69 2, -1)-0.69 2, 1)-0.1 3, -3)-0.08 3, -1)-0.08 3, 1)-0.10 3, 3)
2A ₁ (7F_2)	1064	0.95 2, 0)-0.22 3, -2)+0.22 3, 2)
A ₂ (7F_2)	1226	0.70 2, -2)-0.70 2, 2)+0.06 3, 0)
1B ₂ (7F_3)	1784	-0.11 2, -1)+0.11 2, 2)+0.23 3, -3)+0.64 3, -1)+0.64 3, 1)+0.23 3, 3)+0.14 4, -3)-0.05 4, -1)+0.05 4, 1)+0.14 4, 3)
1A ₂ (7F_3)	1864	0.06 2, -2)-0.06 2, 2)+0.19 3, -2)+0.96 3, 0)+0.19 3, 2)+0.07 4, -4)-0.07 4, 4)
1B ₁ (7F_3)	1887	-0.08 1, -1)+0.08 1, 1)+0.14 3, -3)+0.67 3, -1)-0.67 3, 1)-0.14 3, 3)+0.07 4, -3)-0.12 4, -1)-0.12 4, 1)+0.07 4, 3)
2B ₂ (7F_3)	1953	0.10 1, -1)+0.10 1, 1)-0.10 2, -1)+0.1 2, 2)+0.64 3, -3)-0.24 3, -1)-0.24 3, 1)+0.64 3, 3)+0.11 4, -1)-0.11 4, 1)
2A ₁ (7F_3)	1977	0.19 2, -2)+0.19 2, 2)+0.67 3, -2)-0.67 3, -2)-0.17 4, 0)
2B ₁ (7F_3)	1992	0.10 2, -1)+0.10 2, 1)+0.67 3, -3)-0.15 3, -1)+0.15 3, 1)-0.67 3, 3)+0.11 4, -3)+0.11 4, 3)-0.07 5, -1)+0.07 5, 1)
2A ₂ (7F_3)	2056	0.67 3, -2)-0.26 3, 0)+0.67 3, 2)-0.05 4, -4)+0.11 4, -2)-0.11 4, 2)+0.05 4, 4)-0.06 5, 0)
1A ₁ (7F_4)	2597	0.08 3, -2)+0.08 3, 2)+0.97 4, 0)+0.15 5, -2)-0.15 5, 2)
1B ₁ (7F_4)	2627	-0.05 3, -3)-0.11 3, -1)+0.11 3, 1)+0.05 3, 3)-0.43 4, -3)+0.52 4, -1)+0.52 4, 1)-0.43 4, 3)-0.06 5, -5)+0.06 5, -3)+0.12 5, -1)-0.12 5, 1)-0.06 5, 3)+0.06 5, 5)+0.06 6, -5)+0.06 6, -3)+0.06 6, 3)+0.06 6, 5)
2A ₁ (7F_4)	2820	0.63 4, -4)+0.30 4, -2)+0.30 4, 2)+0.63 4, 4)+0.08 5, -4)-0.08 5, 4)-0.08 6, -4)+0.06 6, -2)+0.06 6, 2)-0.08 6, 4)
1A ₂ (7F_4)	2904	0.08 3, -2)+0.06 3, 0)+0.08 3, 2)+0.55 4, -4)+0.43 4, -2)-0.43 4, 2)-0.55 4, 4)
1B ₂ (7F_4)	2984	-0.06 2, -1)+0.06 2, 1)+0.11 3, -3)-0.07 3, -1)-0.07 3, 1)+0.11 3, 3)+0.16 4, -3)+0.66 4, -1)-0.66 4, 1)-0.16 4, -3)+0.05 5, -5)+0.09 5, -1)+0.09 5, 1)-0.05 5, -5)+0.05 5, 5)+0.06 6, -1)+0.06 6, 1)-0.05 6, 5)
2B ₁ (7F_4)	2997	0.13 3, -3)-0.07 3, -1)+0.07 3, 1)-0.13 3, -3)+0.47 4, -3)+0.44 4, -1)+0.44 4, 1)+0.47 4, 3)-0.23 5, -1)+0.23 5, 1)+0.07 6, -3)+0.07 6, 3)
2B ₂ (7F_4)	3058	0.11 3, -3)+0.10 3, -1)+0.10 3, 1)+0.11 3, 3)+0.66 4, -3)+0.15 4, -1)-0.15 4, 1)-0.66 4, 3)+0.09 5, -5)-0.08 5, -3)+0.06 5, -1)+0.06 5, 1)+0.08 5, 3)+0.09 5, 5)
3A ₁ (7F_4)	3081	0.08 3, -2)-0.08 3, 2)-0.28 4, -4)+0.61 4, -2)+0.18 4, 0)+0.61 4, 2)-0.28 4, 4)-0.07 5, -4)+0.15 5, -2)-0.15 5, 2)+0.07 5, 4)
2A ₂ (7F_4)	3256	-0.08 3, -2)+0.06 3, 0)-0.08 3, 2)-0.55 4, -4)-0.43 4, -2)+0.43 4, 2)+0.55 4, 4)

Table 6 Scalar crystal field strength parameters and maximum splitting energies of the 7F_1 manifold for europium(III) complexes with polycarboxylates (all values are in cm⁻¹)^a

	[Eu(DCTA)] ⁻	[Eu(DPA) ₃] ^{-b}	[Eu(ODA) ₃] ^{-c}	[Eu(EDTA)] ^{-d}	[Eu(phen) ₂] ^{3+e}	[Eu(PU) ₈] ^{3+f}
Site symmetry	C _{2v}	D ₂	D ₃	C _{2v}	D ₂	D ₂
Barycenter 7F_1	393	367	388	380	368.8	359
B ₀ ²	-510	-153	112	-485	355.2	-536.3
B ₂ ²	180	-70	—	89	-116.8	-442.3
N _v	857	267	178	782	563	850
ΔE (exptl.)	160	56	34	161	135	166
ΔE (theo.)	167	52	34	152	110	165

^a The maximum splitting energy was calculated by eqn. (4) with $\alpha = 0.5$. ^b From ref. 14. ^c From ref. 13. ^d The energy parameters will be published elsewhere. ^e [Eu(phen)₂][NO₃]₃ (phen = 1,10-phenanthroline). ^f [Eu(PU)₈][NO₃]₃ [PU = tetrahydro-2(1H)-pyrimidinone].^{6d}

systems. For the other states for which the J mixing is not negligible, the appropriate eigenstates should be employed in eqn. (4).

Emission features

Among the luminescence bands of the europium(III) complex the most striking feature is observed in the ${}^5D_0 \rightarrow {}^7F_2$ transition, which depends on complex stability and structure. This transition is hypersensitive to environment when the ion does not lie on an inversion center. When some water molecules are replaced by DCTA ligand to form the 1:1 Eu^{III}:DCTA complex the oscillator strength of this transition increases to 15.8 times that seen for Eu³⁺(aq). For the other transitions the intensities are enhanced moderately by the complexation with DCTA: 3.0 times for the 590 nm band, 5.2 times for the 650 nm band, and 3.7 times for the 695 nm band.

The ${}^5D_0 \rightarrow {}^7F_1$ transition is observed as strong for most europium(III) complexes since it is allowed by the magnetic dipole moment. If this transition is purely the result of the magnetic dipole moment the intensity should be almost independent of the environment. The increase in the oscillator strength of this transition suggests that the electric dipole

moment may partially contribute to the transition probability *via* the complexation with DCTA. The crystal-field potential produced by the water ligands is weak so that the ${}^5D_0 \rightarrow {}^7F_1$ transition yields a single band peaking at 595 nm. For the 1:1 Eu^{III}:DCTA solution an additional weak band, peaking at 600 nm, appeared on the lower energy side of the 595 nm band. If the appearance of this additional band is associated with the induced electric dipole-moment mechanism then either the B₁ or the B₂ level is responsible for this transition. The simulation in the crystalline state attributes the additional band to the A₁(5D_0) \rightarrow B₁ transition. Furthermore, in the crystalline states, the high-energy side is split into two separate lines, assigned as the A₁(5D_0) \rightarrow A₂ and B₂ transitions, respectively. As discussed, a negative value of B₀² resulted in the A₁(5D_0) \rightarrow A₂ transition in the short wavelength region and the A₁(5D_0) \rightarrow B₂ and B₁ transitions in the long wavelength region.

The relative oscillator strengths (ROS) of the four ${}^5D_0 \rightarrow {}^7F_J$ ($J = 1, 2, 3, 4$) luminescence bands with respect to that of the ${}^5D_0 \rightarrow {}^7F_1$ transition have been reported for [Eu(DPA)₃]³⁻ (DPA = pyridinedicarboxylate) and [Eu(ODA)₃]³⁻ (ODA = oxydiacetate) in single-crystal phases.¹⁴ For the DCTA complex in the crystalline state the relative values for

the three ${}^5D_0 \rightarrow {}^7F_J$ transitions are 0.04 for $J=0$, 3.18 for $J=2$, 0.08 for $J=3$ and 0.51 for $J=4$. A comparison of the ROS for the ${}^5D_0 \rightarrow {}^7F_2$ transitions gives the order of the hypersensitivity as $ODA(ROS = 1.3) < DCTA < DPA(ROS = 4.2)$, which could be related to the order of the chemical stability.

The ${}^5D_0 \rightarrow {}^7F_3$ transition has been observed as very weak for most europium(III) complexes. For the crystalline phase the relative oscillator strength of this transition increased greatly in the DCTA complex, when compared with those of the DPA and ODA complexes ($ROS < 0.04$). The J mixing of the 7F_3 with the other states would possibly enhance the intensity of the ${}^5D_0 \rightarrow {}^7F_3$ transition. Defining the mixing ratio of the J state with a J' state as $R = \sum v_i^2 / \sum \mu_j^2$ (v_i is a coupling constant of component i in the J' state and μ_j is one of the j component in the J state), then using the simulated eigenstates for all levels in the 7F_3 state except the $1A_2$ level R ranges from 0.06 to 0.09. Here, the R of the $1A_2$ level is nearly negligible. These R values are larger than for the DPA complex, of which the maximum value is 0.02. For the DCTA complex the mixing of the 7F_3 state may add an allowed magnetic dipole character to the electric dipole character, which enhances the intensity of the ${}^5D_0 \rightarrow {}^7F_3$ transition.

The ${}^5D_0 \rightarrow {}^7F_4$ transition is sensitive to the ligand environment. For $[Eu(DCTA)]^-$ the intensity of this transition increased moderately. The characteristic feature of this transition can be found in the well separated luminescence lines rather than the enhanced intensity. The C_{2v} crystal-field potential produces the 7 lines allowed by the electric dipole moment. Although the ${}^5D_0 \rightarrow {}^7F_4$ transition does not show apparent sensitivity to the ligand environment, it yields the maximum number of allowed lines.

Conclusion

The crystal structure and the luminescence properties of europium(III) complex with DCTA have been revealed. The Eu^{III} is co-ordinated by N1, N2, O1, O3, O5, O7, OW1 and OW1(a). Here, OW1(a) is superposed onto the OW1 atom by the symmetry transformation $(1-x, 1-y, 1-z)$. Each of the water oxygen atoms co-ordinates two adjacent europium(III) ions resulting in a dimer. In the complex the cyclohexane ring in DCTA has a chair conformation.

The single $[Eu(DCTA)]^-$ crystals produce the 18 characteristic luminescence lines that are responsible for the transitions from the 5D_0 state to the 7F_J ($J=0, 1, 2, 3, 4$) states. These lines are satisfactorily simulated by the crystal-field splitting of Eu^{III} with C_{2v} site symmetry. This indicates that trivalent europium ion can provide very useful luminescence properties for the study of molecular dynamics and structures under specific physical and chemical conditions.

Acknowledgements

This work was supported by the Korean Science and Engineering Foundation (KOSEF 971-0305-038-2).

References

- 1 J.-C. G. Bünzli, *Lanthanide Probes in Life, Chemical and Earth Sciences*, eds. J.-C. G. Bünzli and G. R. Choppin, Elsevier, Amsterdam, Oxford, New York, Tokyo, 1989, ch. 7.
- 2 S. C. Davis and F. S. Richardson, *Inorg. Chem.*, 1984, **23**, 184.
- 3 J.-C. G. Bünzli, P. Froidevaux and C. Piguet, *New J. Chem.*, 1995, **19**, 611.
- 4 O. L. Malta, H. F. Brito, J. F. S. Menezes, F. R. Gonçalves e Silva and S. Alves, Jr., *J. Lumines.*, 1997, **75**, 255.
- 5 W. De W Horrocks, Jr. and D. R. Sudnick, *Acc. Chem. Res.*, 1981, **14**, 384; F. S. Richardson, *Chem. Rev.*, 1982, **82**, 541; D. H. Metcalf, S. W. Snyder, J. N. Demas and F. S. Richardson, *J. Am. Chem. Soc.*, 1990, **112**, 469; L. M. Vallarino, *Handbook on the Physics and Chemistry of Rare Earths*, eds. K. A. Gschneidner, Jr. and Le R. Eyring, North-Holland, Amsterdam, London, New York, Oxford, 1991, vol. 15, ch. 104.
- 6 (a) B. G. Wybourne, *Spectroscopic Properties of Rare Earths*, Wiley, New York, London, Sydney, 1964; (b) C. A. Morrison and R. P. Leavitt, *Handbook on the Physics and Chemistry of Rare Earths*, eds. K. A. Gschneidner, Jr. and Le R. Eyring, North-Holland, Amsterdam, New York, Oxford, 1982, vol. 5, ch. 46; (c) T. D. Hopkins, J. P. Bolender, D. H. Metcalf and F. S. Richardson, *Inorg. Chem.*, 1996, **35**, 5347; (d) Y. Fan and P. Yang, *J. Phys. Chem.*, 1996, **100**, 69.
- 7 W. D'Olieslager and A. Oeyen, *J. Inorg. Nucl. Chem.*, 1978, **40**, 1565.
- 8 C. C. Bryden and C. N. Rellley, *Anal. Chem.*, 1982, **54**, 610.
- 9 G. M. Sheldrick, (a) *Acta Crystallogr., Sect. A*, 1990, **46**, 467; (b) SHELXL 97, Program for Crystal Structure Analysis, Institute fuer Anorganische Chemie der Universitaet, Göttingen, 1998.
- 10 C. K. Johnson, ORTEP, Report ORNL-5138, Oak Ridge National Laboratory, Oak Ridge, TN, 1976.
- 11 R. Reisfeld and C. K. Jorgenson, *Lasers and Excited States of Rare Earths*, Springer, Berlin, Heidelberg, New York, 1977.
- 12 W. T. Carnall, P. R. Fields and K. Rajnak, *J. Chem. Phys.*, 1968, **49**, 4450.
- 13 J.-G. Kang, S.-K. Yoon, Y. Sohn and J.-G. Kim, *J. Bull. Korean Chem. Soc.*, 1997, **18**, 861.
- 14 J.-G. Kim, S.-K. Yoon, Y. Sohn and J.-G. Kang, *J. Alloys Compd.*, 1998, **274**, 1.
- 15 (a) Z. B. Goldschmidt, *Handbook on the Physics and Chemistry of Rare Earths*, eds. K. A. Gschneidner, Jr. and Le R. Eyring, North-Holland, Amsterdam, New York, Oxford, 1978, vol. 1, ch. 1; (b) W. T. Carnall, G. L. Goodman, K. Rajank and R. S. Rana, *J. Chem. Phys.*, 1989, **90**, 3443.
- 16 R. T. Harley, *Spectroscopy of Solids Containing Rare Earth Ions*, eds. A. A. Kaplyanskii and R. M. MacFarlane, North-Holland, Amsterdam, New York, Tokyo, 1987, ch. 9.
- 17 F. K. Andrew and F. S. Richardson, *J. Phys. Chem.*, 1983, **87**, 2557.
- 18 (a) F. Auzel and O. L. Malta, *J. Physique*, 1983, **44**, 201; (b) O. L. Malta, E. Antic-Fidancev, M. Lemaitre-Blaise, A. Milicic-Tang and M. Taibi, *J. Alloy Comp.*, 1995, **228**, 41.

Paper 8/07775D